PHYSICAL REVIEW D **86,** 094021 (2012)

$\gamma^*\gamma \to \pi^0$ transition form factor at low energies from a model-independent approach

Pere Masjuan

Departamento de Física Teórica y del Cosmos and CAFPE, Universidad de Granada, E-18071 Granada, Spain

(Received 14 June 2012; published 15 November 2012)

The recent measured $\gamma^*\gamma \to \pi^0$ transition form factor in the spacelike region by the Belle Collaboration together with the previously published results by CLEO, CELLO, and *BABAR* collaborations, are analyzed using the mathematical theory of Padé approximants. The theory provides a good and systematic description of the low-energy region exemplified here with the extraction of the slope a_π and curvature b_π of the form factor in a model-independent way. Their impact on the pion exchange contribution to the hadronic light-by-light scattering part of the anomalous magnetic moment a_μ is also discussed.

DOI: 10.1103/PhysRevD.86.094021 PACS numbers: 12.38.−t, 12.38.Lg, 12.39.Fe, 13.40.Gp

I. INTRODUCTION

The pion transition form factor (TFF) between a photon and a pion is extracted from the $e^+e^- \to e^+e^-\pi^0$ process, where the π^0 is produced via the two-photon production mechanism. This transition is represented as a function of the photon virtualities as $F_{\pi^0\gamma^*\gamma^*}(q_1^2, q_2^2)$. The TFF is then extracted when one of the electrons is tagged. This electron emits a highly off-shell photon with momentum transfer $q_1^2 \equiv -Q^2$ and is detected, while the other, untagged, is scattered at a small angle and then its momentum transfer q_2^2 is near zero. The pion transition form factor is then defined as $F_{\pi^0\gamma^*\gamma^*}(-Q^2, 0) \equiv F_{\pi^0\gamma^*\gamma}(Q^2)$.

The TFF was measured in the CELLO [1] and CLEO [2] experiments in the momentum transfer ranges 0.7–2.2 GeV^2 and 1.6–8.0 GeV^2, respectively. At 2009, the *BABAR* Collaboration extended these measurements in the Q^2 range from 4 to 40 GeV^2 [3]. And recently [4], the Belle Collaboration has measured the form factor in the same *BABAR*'s energy region with slightly different results on the high-energy region.

At low transferred momentum, the TFF can be described by the following expansion:

$$F_{\pi^0\gamma^*\gamma}(Q^2) = a_0\left(1 + a_\pi \frac{Q^2}{m_\pi^2} + b_\pi \frac{Q^4}{m_\pi^4} + \mathcal{O}(Q^6)\right), \quad (1)$$

where the parameter a_0 can be determined from the axial anomaly [5,6] in the chiral limit of QCD, $a_0 = \frac{1}{4\pi^2 f_\pi}$ with f_π the pion decay constant.

The parameter a_π, the slope of the TFF, was measured by [7–9], with the results $a_\pi = -0.11(3)(8)$, $a_\pi = 0.026(24)(48)$, and $a_\pi = 0.025(14)(26)$, respectively (the first error is statistic and the second systematic). The CELLO Collaboration estimated a_π to be $a_\pi = 0.0326(26)_{\text{stat}}(26)_{\text{sys}}$ in Ref. [1] using an extrapolation from the region of large spacelike momentum transfer, assuming a vector meson dominance (VMD) and using at zero transferred momentum the current experimental value for the partial decay width $\Gamma_{\pi^0\to\gamma\gamma}$ [which, as we will see later, is related to $F_{\pi^0\gamma^*\gamma}(Q^2 = 0)$, the axial anomaly]. The KTeV Collaboration also predicted $a_\pi = 0.040(40)$ through a model-dependent fit to timelike data [10]. The CELLO prediction, however, dominates the number quoted by the PDG [11] since the direct measurements are less precise.

A VMD fit to all of the available data (CELLO, CLEO, *BABAR*, and Belle) would yield $a_\pi = 0.0275(5)$ with a $\chi^2/\text{d.o.f.} = 2.4$ (d.o.f. meaning "degrees of freedom"), which means a 1.4 standard deviation from the CELLO result. This result suggests that the high-energy data may be important for determining low-energy properties of the TFF.

One immediately comes to the question of how to improve the quality of the fits to stabilize the predicted result and also of how to assign a systematic error to the fit procedure.

In Ref. [12] it was suggested that the VMD is a first step of a sequence of particular rational approximations called Padé approximants (PA). In that reference, it was also suggested that using Padé approximants as fitting functions to analyze the pion vector form factor in the spacelike region, one can go beyond the VMD in a systematic approximation.

In the TFF case, this fact is of particular interest since the data from the *BABAR* Collaboration cannot be easily accommodated in the VMD picture. With the help of these rational approximants, one could reach systematically the intermediate and high-energy experimental data, producing, at the same time, accurate results for the slope and curvature of the TFF at low energies.

The Padé techniques provide a simple, model-independent, and systematic method of fitting data with a larger range of convergence than the simple polynomial fit or a VMD-like fit (such as the one used by the CELLO Collaboration to extract the a_π parameter). Given a function $f(z)$ defined in the complex plane, the PA $P_M^N(z)$ are ratios of two polynomials $R_N(z)$ and $Q_M(z)$ (with

*masjuan@ugr.es

degree N and M, respectively), the coefficients of which exactly coincide with the coefficients of the Taylor expansion of $f(z)$ up to the highest order; i.e., $f(z) - P_M^N(z) = \mathcal{O}(z^{N+M+1})$.

The PA method also provides an estimation of a systematic error and could also be used to evaluate the impact of the vector excitations in the process considered. The techniques described here were also applied to the search for resonance poles in Ref. [13].

There are several types of PA but, as pointed out in Ref. [12], the analytic properties of the function to be approximated determine which PA should be used. The timelike region is largely dominated by the ρ-meson contribution. The natural choice seems to be a $P_1^L(Q^2)$. On the other hand, since it is well known [14] that the TFF behaves like $1/Q^2$ at very large energies, one could try to incorporate this information by considering a $P_{N+1}^N(Q^2)$.

For explanatory reasons we show here how to construct a $P_1^L(Q^2)$ approximant [a $P_{N+1}^N(Q^2)$ is more involved and less illustrative].

Given a function $f(z)$ defined in the complex plane, a Padé approximant P_1^L is defined [15], without any loss of generality, by

$$P_1^L(z, z_0) = \sum_{k=0}^{L-1} a_k (z - z_0)^k + \frac{a_L (z - z_0)^L}{1 - \frac{a_{L+1}}{a_L}(z - z_0)}, \qquad (2)$$

where the coefficients a_k are the Taylor coefficients of the corresponding $f(z)$ function that has been approximated.

Equation (2) shows that the pole s_p of each P_1^L is determined by the ratio $s_p = a_L/a_{L+1}$.

The TFF seems to be well described by the simple VMD ansatz. VMD relies on the accurate knowledge of the light meson spectra. When the spectral information is given in advance, one should also take advantage of that information and consider other kinds of rational approximants. These are the Padé-type approximants (PTAs). In the PTAs the poles of the Padé are fixed to certain values (in our case, the resonances of the spectrum).

The simplest PTA sequence incorporates the lowest resonance, the M_ρ, and it is called T_1^L. The famous VMD ansatz is nothing but the simplest PTA, the T_1^0 approximant.

The purpose of this paper is twofold: First, we want to extract the slope and the curvature of the transition form factor using a sequence of P_1^L approximants as fitting functions to the available experimental data. We demand an assignment of a systematic error to our predictions. Second we estimate the impact of our results on the light-by-light (LBL) contribution to the hadronic process on the muon g-2. We also comment in passing on the recent proposal to measure the transition form factor at low energy using the BESIII experiment.

We proceed as follows: In Sec. II we study the reliability of the PA method at fitting functions and then proceed in Sec. III to analyze the real data. In Sec. IV we consider the impact of the previous result on the LBL contribution to the muon g-2. We finally collect all of the results in the Conclusions section.

II. TESTING THE METHOD WITH A MODEL

Before applying the method to the experimental data to extract the slope and the curvature of the TFF, we want to test its reliability with a particular model. Since it has not been possible to describe rigorously the TFF from basic principles, several models have been developed during the last years with the purpose of analyzing the spacelike data to extract fundamental QCD properties. In these Refs. [16–38], we try to summarize the large effort made toward this purpose.

Considering the variety of models, we examine three of them instead of just one. We think these three are representative of the large amount of work done in this respect. Since our intent is to show the properties of our method, the selected models should describe well the experimental data but keep the complexity at a manageable level. This exercise will also provide a way to estimate the systematic error of our approximations.

For ease of reading, we comment here about the first model and relegate the other two to the Appendix.

The first model considered is motivated by a quark model (e.g., Refs. [19–21,36]; see also Ref. [28] for other $\log(Q^2/M^2)$ related models), although it can also be inspired by the lowest order perturbative QCD (pQCD) with a flat pion distribution amplitude (see, for example, Ref. [20]) or even by the *BABAR* fitting function [3]. We named this model the "log model":

$$F_{\pi^0\gamma^*\gamma}(Q^2) = \frac{M^2}{4\pi^2 f_\pi Q^2} \log\left(1 + \frac{Q^2}{M^2}\right), \qquad (3)$$

with $M^2 = 0.6$ GeV^2 and $f_\pi = 92$ MeV.

Expanding $F_{\pi^0\gamma^*\gamma}(Q^2)$ in Eq. (3) in powers of Q^2, we obtain

$$F_{\pi^0\gamma^*\gamma}(Q^2) = a_0 - a_1 Q^2 + a_2 Q^4 - a_3 Q^6 + \mathcal{O}(Q^8), \qquad (4)$$

with known values for those a_i coefficients (in particular $a_0 = \frac{1}{4\pi^2 f_\pi}$), as shown in the last column of Table I.

In order to illustrate the utility of the PA as a fitting function, we simulate the situation of the experimental data [1–4] with the model by considering the function Eq. (3) evaluated at 22 points in the region $0.7 \le Q^2 \le 5.5$ GeV^2, 16 points in the region $5.5 \le Q^2 \le 12.5$ GeV^2, and 14 more points in the region $12.5 \le Q^2 \le 35$ GeV^2. On top of these sets of data points, we add the value of $F_{\pi^0\gamma\gamma}(0, 0) = \frac{1}{4\pi^2 f_\pi}$. All of these data points have zero error because we want to obtain a pure systematic error on our fitting functions.

We construct a sequence of $P_1^L(Q^2)$ approximants with unknown coefficients, as defined in Eq. (2), and then we fit

TABLE I. a_0, a_1, and a_2 low-energy coefficients of the log model in Eq. (3), fitted with a $P_1^L(Q^2)$ and its exact values (last column). We also include the prediction for the pole of each $P_1^L(Q^2)$ (s_p) to be compared with the lowest-lying meson in the model.

	P_1^0	P_1^1	P_1^2	P_1^3	P_1^4	P_1^5	$F_{\pi^0\gamma^*\gamma}$ (exact)
a_0 (GeV^{-1})	0.2556	0.2694	0.2734	0.2746	0.2751	0.2752	0.2753
a_1 (GeV^{-3})	0.1290	0.1716	0.1935	0.2051	0.2124	0.2166	0.2294
a_2 (GeV^{-5})	0.0651	0.1147	0.1492	0.1725	0.1898	0.2013	0.2549
$\sqrt{s_p}$ (GeV)	1.41	1.22	1.14	1.09	1.05	1.03	0.77

the set of data which yields a predictions for the a_i coefficients. The results are shown in Table I, where we go up to the P_1^5. The first P_1^0 has only two parameters (a_0 and a_1), and then a_2 is not fitted but predicted through expansion. We also include in this table the position of the pole of each PA. The reader should notice how these poles, although showing a convergence pattern, differ from the lowest-lying vector mass used in the model of Eq. (3).[1]

As expected [12], the sequence of PAs converges to the exact result in a hierarchical way (much faster for a_0 than for a_1 and so on), achieving with the last PA P_1^5 a relative error of 0.04%, 5.6%, and 21.0% for a_0, a_1, and a_2 respectively.

Similar results can be found by using a sequence of PTAs as fitting function, as we wrote in the introduction. Thus, fixing the pole of the T_1^L at $s_p = M^2 = (0.77)^2$ GeV^2, we obtain for the T_1^5 a relative error of 3%, 34%, and 92% for a_0, a_1, and a_2, respectively. These results could be easily improved if instead of fixing the pole of our PTA on the starting point of the branch cut, i.e., at $s_p = (0.77)^2$ GeV^2, we fix it at a different $s_p > (0.77)^2$ GeV^2. For example, if $s_p = 1$ GeV^2 (value motivated by the result obtained with the previous P_1^5) the relative errors turn out to be 0.15%, 2.3%, and 14.4% for a_0, a_1, and a_2, respectively. Since the PTA's predictions are very similar to PA's ones, we do not show explicitly the corresponding table. This simple exercise shows that fixing the pole of our approximant to the physical resonance, as in the VMD case, might not be the best strategy to follow for low-energy constant predictions, as extensively studied in Ref. [39].

The nice convergence pattern shown by our PA sequence should not be a surprise, since it turns out that our model Eq. (3) is a Stieltjes function. Thus, the convergence of the PA sequences is guaranteed by Padé theory [40].

On the other hand, a possibility has been recently considered in Ref. [41] for the KLOE-2 experiment at Frascati to measure the TFF at very low energies in the spacelike region (for $0.01 < Q^2 < 0.1$ GeV^2) and the width $\Gamma_{\pi^0\to\gamma\gamma}$ at the percent level. This new low-energy data may reduce our systematic error for the PA P_1^5 to 4.2% and 18% for a_1 and a_2, respectively. An even better result might be obtained when the BES-III experiment at the e^+e^- collider BEPC-II in Beijing will cover a range from low-energy up to CELLO energies, i.e., up to $Q^2 \sim 0.7$ GeV^2 (which will turn out to have systematic errors less than 3% and 15% for a_1 and a_2, respectively, considering the feasibility study for BES-III performed in Ref. [42]). Indeed, the $\gamma\gamma$ physics program at BES-III for the measurement of pseudoscalar TFFs will allow us to cover a wide Q^2 range below 10 GeV^2, the gap between KLOE-2 and CLEO experiments.

We analyze two more models in the Appendix using the same technique explained here, and the similar results obtained with the three of them give us confidence in our fit procedure. This exercise allows us to assign a systematic error for each element on the PA and the PTA sequences. To ascribe a particular (and conservative) systematic error, and taking into account that we do not know the structure of the whole TFF, we select the worst of the three cases as a guide. For PA P_1^5, 5.6% and 21% are the relative systematic errors for a_1 and a_2, respectively; for PTA T_1^5, they are 5.4% and 20%.

III. FITS TO REAL DATA

With all the tools developed so far, we can now proceed to analyze the real TFF. For this purpose we use all the available experimental data in the spacelike region, which

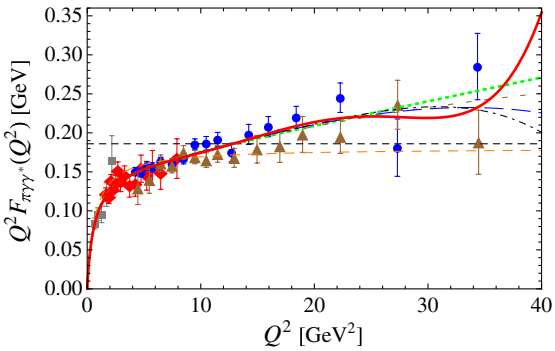

FIG. 1 (color online). The P_1^L sequence compared with the $\gamma^*\gamma \to \pi^0$ transition form factor data from CELLO (gray squares) [1], CLEO (red diamonds) [2], *BABAR* (blue circles) [3], and Belle (brown triangles) [4]: P_1^0 (orange dashed), P_1^1 (green dotted), P_1^2 (brown short-dashed), P_1^3 (blue long-dashed), P_1^4 (black dot-dashed), and P_1^5 (red solid). The black dashed line indicates the pQCD result.

[1]The model of Eq. (3) has a branch cut starting at $Q^2 \leq -M^2$.

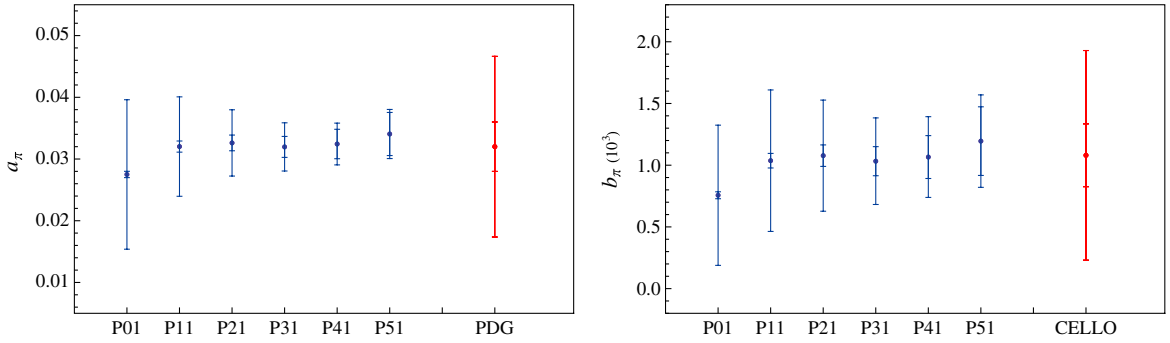

FIG. 2 (color online). a_π (left) and b_π(right) predictions with the P_1^L up to $L = 5$. The internal band is the statistical error from the fit and the external one is the combination of statistical and systematic errors determined in the previous section.

may be found in Refs. [1–4], and also the recent measurement of the $\Gamma_{\pi^0\to\gamma\gamma}$ decay width by the PrimEx Collaboration [43].

The form factor for real photons is related to the $\pi^0 \to \gamma\gamma$ decay width:

$$F^2_{\pi^0\gamma\gamma}(q_1^2 = 0, q_2^2 = 0) = \frac{4}{\pi\alpha^2 m_\pi^3}\Gamma_{\pi^0\to\gamma\gamma}, \qquad (5)$$

with $\alpha = \alpha_{em} = 1/137.0356$.

The experimental world average collected in the PDG tables [11] is $\Gamma^{\rm PDG}_{\pi^0\to\gamma\gamma} = 7.74 \pm 0.48$ eV, although we use here the PrimEx Collaboration result [43] that has significantly improved the accuracy using a Primakoff effect experiment at JLab, reporting the value $\Gamma_{\pi^0\to\gamma\gamma} = 7.82 \pm 0.14 \pm 0.17$ eV.

A. Fits with the rational approximants

The fits with the P_1^L sequence to the spacelike data points in Refs. [1–4] determine those a_k coefficients that best interpolate them. As always, when fitting experimental data, one should find a compromise between the increase of fit errors and decrease of systematic ones when increasing the order L of the P_1^L. Figure 1 shows the experimental data obtained by CELLO (gray squares),[2] CLEO (red diamonds), *BABAR* (blue circles), and Belle (brown triangles), together with the pQCD prediction (horizontal black dashed line). The red curve in Fig. 1 is our best approximant, the P_1^5.

In Fig. 2 we show the results for the prediction of the slope and curvature parameters a_π and b_π with the P_1^L up to $L = 5$. Approximants with $L > 5$ have the new coefficients compatible with zero and then do not introduce new information with respect to P_1^5. The internal errors shown in Fig. 2 are only statistical; the external ones are a quadratic combination of statistical and systematic errors, the latter determined in the previous section. For completeness we also ascribe a 45% systematic error to the PDG slope value.[3] The curvature parameters have never been measured, so for ease of comparison we expand the VMD fit used by the CELLO Collaboration up to that order with the corresponding systematic error.

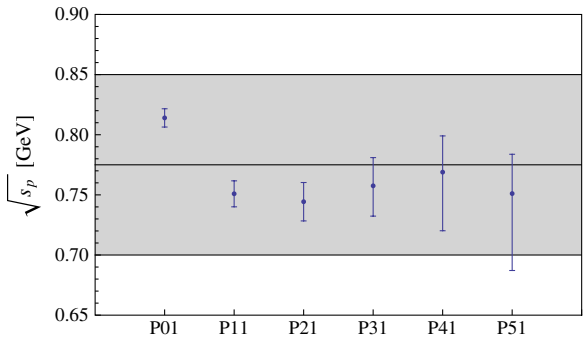

FIG. 3 (color online). Position of the pole $\sqrt{s_p}$ for the different P_1^L. For comparison, we also show (gray band) the range $M_\rho \pm \Gamma_\rho/2$ corresponding to the physical ρ-meson value.

As expected from the models studied, we see in these figures a nice convergence pattern for both a_π and b_π.

The PA P_1^5 yields

$$a_\pi = 0.0340(35)_{\rm stat}(19)_{\rm sys}, \qquad (6)$$

and

$$b_\pi = 1.20(28)_{\rm stat}(25)_{\rm sys} \times 10^{-3}, \qquad (7)$$

with a $\chi^2/\text{d.o.f.} = 0.80$, where the systematic error is estimated from the previous section (5.6% for a_π and 21% for b_π). We also extract the position of the PA pole $s_p = a_L/a_{L+1}$. This ratio is shown in Fig. 3, together with a band corresponding to the physical value $M_\rho \pm \Gamma_\rho/2$, where $M_\rho = 0.7755$ GeV and $\Gamma_\rho = 0.155$ GeV is believed to be the dominant resonance contribution. For

[2]CELLO data points D_i are extracted from Ref. [1] using the following normalization: $D_i = (\frac{64\pi N_i}{(4\pi\alpha)^2 m_\pi^2})^{1/2}$, with the $N_i = \frac{F^2(Q_i^2)m_\pi^3}{64\pi}$ provided in that reference and $\alpha = 1/137.036$.

[3]Again, this systematic error is obtained by comparing the VMD result with the exact ones in Tables I, IV, and V.

TABLE II. Slope and curvature of the TFF predictions with a P_1^5 with different sets of data.

Data	a_π	$(10^3)b_\pi$	$\sqrt{s_p}$	χ^2/d.o.f.
All	0.0340(35)	1.20(28)	$0.75^{+0.03}_{-0.06}$	0.80
CELLO+CLEO+*BABAR*	0.0348(39)	1.26(32)	$0.73^{+0.04}_{-0.06}$	0.61
CELLO+CLEO+Belle	0.0326(39)	1.08(30)	$0.76^{+0.05}_{-0.06}$	0.49

TABLE III. Slope of the TFF prediction with different sets of data, as described in the main text.

	Best PA	a_π	χ^2/d.o.f.
Data up to 10 GeV^2	P_1^3	0.0364(51)	0.53
Data up to 20 GeV^2	P_1^4	0.0327(35)	0.69
All	P_1^5	0.0340(35)	0.80

the P_1^5, the pole is located at $\sqrt{s_p} = 0.75^{+0.03}_{-0.06}$ GeV, well within this band.

It is interesting to notice the slightly larger results for the slope obtained with P_1^L with $L > 1$, manifesting the need of a systematic procedure for going beyond VMD. It turns out that the larger L is, the larger the sensibility of the P_1^L to the high-energy data. In this respect, the recent Belle data are crucial to obtain an accurate low-energy prediction, since up to now *BABAR* data were dominating the high-energy region (see, for example, Ref. [13] for a preliminary study without Belle data).

Our final result is a fit to all of the available data, but for a deeper understanding of PA as fitting functions for high-energy data, we consider two different scenarios where first no Belle data are considered and second no *BABAR* data are considered (Table II). Surprisingly enough, the results shown in Table II (where "All" stands for all of the available data) are nicely compatible within errors although with slightly different central values. All of the results are obtained with a P_1^5.

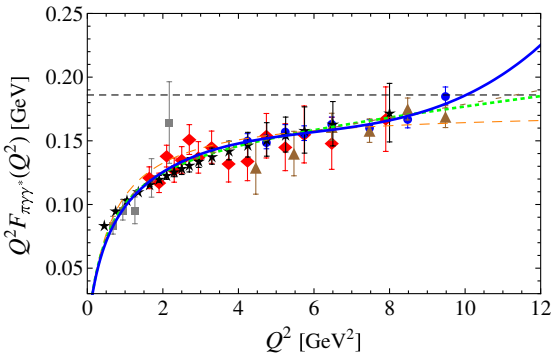

FIG. 4 (color online). The P_1^L sequence compared with the $\gamma^*\gamma \to \pi^0$ transition form factor data up to 10 GeV^2 [1–4,42]: P_1^0 (orange dashed), P_1^1 (green dotted), P_1^2 (brown short-dashed), P_1^3 (blue solid). The black dashed line indicates the pQCD result.

Finally, we want to apply a last test of robustness to the method, which is that fits to subsets of data should return compatible results; i.e., fitting data up to 10 GeV^2, up to 20 GeV^2, and up to 36 GeV^2 (all of the data) should be the same (unless there are unknown problems with the data such as normalization or systematics). The results are shown in Table III, where we also indicate the best P_1^L that fits the particular subset of data. These results are nicely compatible; otherwise we should take the difference as a new source of systematic error.

For illustrative purposes, we show in Fig. 4 the result when fitting data up to 10 GeV^2. In this case we include also the feasibility study for BES-III experiment performed in Ref. [42]. With a P_1^3 we obtain[4] $a_\pi = 0.036(6)$ and $b_\pi = 1.41(65)$, where the errors are statistical and systematical with χ^2/d.o.f. $= 0.53$, to be compared with the results in Table II. In this scenario, the pole of the P_1^3 is located at $\sqrt{s_p} = 0.73^{+0.09}_{-0.05}$ GeV.

B. Other Padé approximants

1. P_2^L Padé approximants

The experimental data so far considered range up to 36 GeV^2 then a natural extension of the previous analysis would include higher resonances, although the form factor is believed to be dominated by the $\rho(770)$ meson. In such a way, the consideration of two-pole P_2^L will give us a way to assess any possible systematic bias in our P_1^L analysis.

In this case our best approximant is the P_2^3. This approximant yields

$$a_\pi = 0.0324(20) \quad \text{and} \quad b_\pi = 1.07(15) \times 10^{-3}, \tag{8}$$

with a χ^2/d.o.f. $= 0.71$, nicely compatible with our previous determination in Eqs. (6) and (7). Despite this result, the poles of that approximant are located at $s_{p1} = 0.53(6) - i0.01(1)$ and $s_{p2} = 0.56(2) + i0.01(1)$, where we can see a certain parameter space region where the poles may eventually become complex-conjugated.[5]

2. T_1^L Padé-type approximants

On the other hand, since the value of the physical ρ-meson mass is well known, it is natural to attempt to

[4]PA with larger L do not introduce new information. BES-III data will be crucial to improve on this result.

[5]Complex-conjugate to render the approximant real.

include this information in our analysis through the PTAs. We have seen in the previous section, however, that locating the pole of a PTA exactly at the physical counterpart is not the best strategy. In fact, we learned that $s_p > M_\rho^2$, but it is not clear which particular value we should use. To evaluate a possible systematic error in this choice, we range the PTA pole in between the band drawn by the PA results in Fig. 3; i.e., $\sqrt{s_p} = 0.73$–0.83 GeV.

With a T_1^L sequence, we go up to T_1^5 and obtain also a nice and smooth convergence pattern for both a_π and b_π parameters. With our best PTA, we obtain

$$a_\pi = 0.0302(28) \text{ and } b_\pi = 0.92(18) \times 10^{-3}, \quad (9)$$

with a $\chi^2/\text{d.o.f.} = 0.78$–$0.87$, where the errors are mainly the systematics of the pole range.

3. P_{N+1}^N Padé Approximants

As suggested in the Introduction, we may attempt to include the asymptotic behavior of the TFF [14] in our fits by considering a P_{N+1}^N sequence. With these approximants we can go up to the P_3^2, which yields

$$a_\pi = 0.0331(45) \text{ and } b_\pi = 1.11(27) \times 10^{-3}, \quad (10)$$

with a $\chi^2/\text{d.o.f.} = 0.73$.

The P_3^2 approximant has the right falloff as Q^{-2}, but the corresponding coefficient (which reads 0.17 ± 1.8 GeV) is not correctly predicted due to its large statistical error. This asymptotic coefficient is known to be $2f_\pi$ by first principles [14]. It seems logical to try to include this information on the P_3^2. Using the asymptotic coefficient when constructing the P_3^2, we obtain a constrained approximant called $P_3'^2$ which yields, after fitting the TFF data, for the low-energy coefficients,

$$a_\pi = 0.0332(25) \text{ and } b_\pi = 1.13(19) \times 10^{-3}, \quad (11)$$

with a $\chi^2/\text{d.o.f.} = 0.70$.

It is remarkable that these results for the $P_3'^2$, which make use of all of the experimental data and the asymptotic limit at once, are nicely compatible with all of the previous results. This approximant seems to suggest that the scale where the pQCD should be applied is much further away than the last *BABAR* and Belle data points.

C. Final result

The results shown in Eqs. (6)–(11) agree quite well. Combining them, our final weighted average result yields

$$a_\pi = 0.0324(12)_{\text{stat}}(19)_{\text{sys}}, \quad (12)$$

and

$$b_\pi = 1.06(9)_{\text{stat}}(25)_{\text{sys}} \times 10^{-3}, \quad (13)$$

to be compared with other theoretical determinations: from a Regge analysis, $a_\pi = 0.032(1)$ [17]; from ChPT at the loop level with $\mu = M_\rho$, $a_\pi = 0.036$ [44]; from a study of the Dalitz decay $\pi^0 \to e^+e^-\gamma$, $a_\pi = 0.029(5)$ [45]; from a hard-wall holographic model of QCD, $a_\pi \approx 0.031$ [46] and $a_\pi \approx 0.035$ [47]; from a soft-wall holographic model of QCD, $a_\pi = 0.024(5)$ [48][6]; and finally from the compilation of holographic models in Ref. [49], $a_\pi = 0.031(6)$, where the error is estimated by the spread of the different results obtained from these models.

In the next section, we explore possible consequences of our final results in Eqs. (12) and (13) on the light-by-light scattering contribution to the anomalous magnetic moment of the muon.

IV. IMPLICATIONS ON THE HADRONIC LIGHT-BY-LIGHT CONTRIBUTION TO THE $(g\text{-}2)_\mu$

We can use the results in Eqs. (12) and (13) to constrain any model that estimates the pion-exchange piece to the light-by-light scattering contribution to the $(g\text{-}2)_\mu$, the $a_\mu^{LBL;\pi^0}$ term. As an example, we consider the so called LMD + V model (defined in Ref. [50]) to account for that contribution:

$$F_{\pi^0\gamma^*\gamma^*}^{LMD+V}(Q_1^2, Q_2^2) = \frac{f_\pi}{3} \frac{-Q_1^2Q_2^2(Q_1^2+Q_2^2) + h_1(Q_1^2+Q_2^2)^2 + h_2Q_1^2Q_2^2 - h_5(Q_1^2+Q_2^2) + h_7}{(Q_1^2+M_{V_1}^2)(Q_1^2+M_{V_2}^2)(Q_2^2+M_{V_1}^2)(Q_2^2+M_{V_2}^2)}. \quad (14)$$

The TFF is related to the LMD + V model Eq. (14) when one of the photons on the latter is on shell. That means we cannot fix all of the free parameters (h_i, with $i = 1, 2, 5, 7$, and M_{V_1}, M_{V_2}) on this LMD + V model at once. We need more information, for example, from the high-energy region ($Q^2F_{\pi^0\gamma^*\gamma}(Q^2, 0) = 2f_\pi$; see Ref. [14]). If we match the high-energy limit, we find $h_1 = 0$ and $h_5 = -6M_{V_1}^2M_{V_2}^2$. The axial anomaly on the low-energy limit fixes $h_7 = -\frac{N_c}{4\pi^2 f_\pi^2} M_{V_1}^4 M_{V_2}^4$. With these results and $h_2 = 0$ as suggested in Ref. [50], we can use the slope and the curvature of the TFF to fix M_{V_1} and M_{V_2}. We find $M_{V_1}^2 = 0.33(11)$ GeV^2 and $M_{V_2}^2 = 0.94^{+0.99}_{-0.25}$ GeV^2 and we obtain $a_\mu^{LBL;\pi^0} = 5.4(5) \times 10^{-10}$.

[6]This number is obtained through the large-N_c limit relation $C_{22}^W = \frac{a_\pi N_c}{64\pi^2 m_\pi^2}$ [45] with $C_{22}^W = 6.3 \times 10^{-3}$ obtained in Ref. [48]. Indeed, with our final value for a_π, we predict $C_{22}^W = 8.4(9) \times 10^{-3}$ GeV^{-2}.

V. CONCLUSIONS

In this paper, we analyzed the collection of all of the experimental data on the $\pi^0\gamma^*\gamma$ transition form factor at low energies with a model-independent approach based on Padé approximants, and we obtain the slope $a_\pi = 0.0324(12)_{\rm stat}(19)_{\rm sys}$ and curvature $b_\pi = 1.06(9)_{\rm stat} \times (25)_{\rm sys} \times 10^{-3}$ of the form factor. The method is simple and systematic, and it provides a model-independent estimation of all of the systematic errors. We analyzed the impact at low energy of the Belle and *BABAR* high-energy data and also the future BES-III data. We also evaluate the implications of these results on the pion-exchange contribution on the light-by-light scattering part of the anomalous magnetic moment of the muon. Using the well-known $LMD + V$ parametrization and the Padé theory techniques, we estimate that contribution to be $a_\mu^{LbyL;\pi^0} = 5.4(5) \times 10^{-10}$.

ACKNOWLEDGMENTS

We thank F. Cornet, R. Escribano, A. Nyffeler, E. R. Arriola, and V. Savinov for discussions, B. Kloss, E. Prencipe, and M. Vanderhaeghen for providing us with the feasibility study at the BES-III experiment, and also F. Cornet and E. R. Arriola for a critical reading of the manuscript. This work has been supported by MICINN, Spain (FPA2006-05294), the Spanish Consolider-Ingenio 2010 Programme CPAN (CSD2007-00042) and by Junta de Andalucía (Grants No. P07-FQM 03048 and No. P08-FQM 101).

APPENDIX

For completeness we also studied two more models for the $F_{\pi^0\gamma^*\gamma^*}(q_1^2, q_2^2)$. The first is based on the Regge theory and the second on the light-front holographic QCD. After generating a set of zero error data points for each model, we fit the data with $P_1^L(Q^2)$ and $T_1^L(Q^2)$ sequences.

1. Regge model

We consider first a Regge model based on the large-N_c limit, N_c being the number of colors (see, for example, Refs. [16,17,30,35], where similar large-N_c models are used to fit the available data directly). In this limit, the vacuum sector of QCD becomes a theory of infinitely many noninteracting mesons and the propagators of the hadronic amplitudes are saturated by infinitely many sharp meson states. In the particular case below, the pion couples first to a pair of vector mesons V_ρ and V_ω, which then transform into photons. Thus, we have

$$F_{\pi^0\gamma^*\gamma^*}(q_1^2, q_2^2) = \sum_{V_\rho, V_\omega} \frac{F_{V_\rho}(q_1^2) F_{V_\omega}(q_2^2) G_{\pi V_\rho V_\omega}(q_1^2, q_2^2)}{(q_1^2 - M_{V_\rho}^2)(q_2^2 - M_{V_\omega}^2)} + (q_1 \leftrightarrow q_2), \tag{A1}$$

where F_{V_ρ} and F_{V_ω} are the current-vector meson couplings and $G_{\pi V_\rho V_\omega}$ is the coupling of two vector mesons to the pion. The dependence on the resonance excitation number n is the following:

$$M_{V_\rho}^2 = M_{V_\omega}^2 = M^2 + n\Lambda^2, \quad \text{and} \quad F_{V_\rho} = N_c V_\omega \equiv F. \tag{A2}$$

The combination of sums in Eq. (A1) can be expressed in terms of the digamma function $\psi(z) = \frac{d}{dz}\log\Gamma(z)$:

$$\begin{aligned} F_{\pi^0\gamma^*\gamma^*}(q_1^2, q_2^2) &= F_{\pi^0\gamma^*\gamma^*}(Q^2, A) \\ &= \frac{c}{N_c A Q^2}\left[\psi\left(\frac{M^2}{\Lambda^2} + \frac{Q^2(1+A)}{2\Lambda^2}\right)\right. \\ &\quad \left. - \psi\left(\frac{M^2}{\Lambda^2} + \frac{Q^2(1-A)}{2\Lambda^2}\right)\right], \end{aligned} \tag{A3}$$

where $Q^2 = -(q_1^2 + q_2^2)$, $A = \frac{q_1^2 - q_2^2}{q_1^2 + q_2^2}$, and c a constant.

To reassemble the physical case, we consider $N_c = 3$, $\Lambda^2 = 1.3\ \text{GeV}^2$ (as suggested by the recent light nonstrange $q\bar{q}$ meson spectrum analysis [51]), $A = 1$ (which means $q_2^2 = 0$), $M^2 = (0.8)^2\ \text{GeV}^2$, and the constant c in such a way that the anomaly $F_{\pi^0\gamma\gamma}(0,0) = \frac{1}{4\pi^2 f_\pi}$ is recovered.

Equations (A1) and (A3) use the large-N_c and chiral limits and thus have an analytic structure in the complex momentum plane which consists of an infinity of isolated poles but no branch cut (as does the log model of Sec. II); i.e., they become meromorphic functions. As such, they have a well-defined series expansion in powers of momentum around the origin with a finite radius of convergence given by the first resonance mass. It is well known [52] and largely explored in the context of large N_c [39,53] that the convergence of any near diagonal PA sequence to the original function for any finite momentum, over the whole complex plane (except perhaps in a zero-area set), is guaranteed.

For meromorphic functions such as Eqs. (A1) and (A3), another important result of Padé theory applies here: the Montessus de Ballore's theorem [13,15], which states that given a certain analytic function $f(z)$ at the origin which is meromorphic with exact M poles in a certain disk on the complex plain, the sequence of PAs converges uniformly to $f(z)$. In practice, provided M is known ($M = 1$ in our case), the Montessus' theorem asserts convergence for the sequence of M-pole Padé approximants P_M^L. These convergence theorems are confirmed by the good results collected in Table IV, where after generating a set of zero-error data points with the model of Eq. (A3), we fit them with the PA sequence and obtain the predictions for the a_i coefficients.

With the PA P_1^5 we obtain a relative error of 0.02%, 2.9%, and 9.4% for a_0, a_1, and a_2, respectively. The

TABLE IV. a_0, a_1, and a_2 low-energy coefficients of the Regge model in Eq. (A3), fitted with a $P_1^L(Q^2)$ and its exact values (last column). We also include the prediction for the pole of each $P_1^L(Q^2)$ (s_p) to be compared with the lowest-lying meson in the model.

	P_1^0	P_1^1	P_1^2	P_1^3	P_1^4	P_1^5	$F_{\pi^0\gamma^*\gamma}$ (exact)
a_0 (GeV^{-1})	0.2672	0.2730	0.2746	0.2751	0.2752	0.2753	0.2753
a_1 (GeV^{-3})	0.2662	0.3121	0.3338	0.3457	0.3529	0.3571	0.3678
a_2 (GeV^{-5})	0.2652	0.3600	0.4244	0.4616	0.4868	0.5030	0.5550
$\sqrt{s_p}$ (GeV)	1.00	0.92	0.87	0.86	0.85	0.84	0.80

TABLE V. a_0, a_1, and a_2 low-energy coefficients of the holographic model in Eq. (A4), fitted with a $P_1^L(Q^2)$ and its exact values (last column). We also include the prediction for the pole of each $P_1^L(Q^2)$ (s_p) to be compared with the lowest-lying meson in the model.

	P_1^0	P_1^1	P_1^2	P_1^3	P_1^4	P_1^5	$F_{\pi^0\gamma^*\gamma}$ (exact)
a_0 (GeV^{-1})	0.2791	0.2774	0.2764	0.2759	0.2756	0.2754	0.2753
a_1 (GeV^{-3})	0.3571	0.3362	0.3213	0.3108	0.3033	0.2986	0.2856
a_2 (GeV^{-5})	0.4567	0.4031	0.3643	0.3358	0.3148	0.3009	0.2535
$\sqrt{s_p}$ (GeV)	0.88	0.91	0.94	0.96	0.98	1.00	1.16

inclusion of the feasibility study at BES-III [42] decreases the error down to 2.4% and 7.9% for a_1 and a_2, respectively. With a PTA sequence the results return 0.02%, 0.7%, and 0.8% for a_0, a_1, and a_2, respectively, when the PTA pole is located at $s_p = 0.70$ GeV^2.

2. Holographic model

Finally, as a third model we analyze a simple holographic confining model presented in Ref. [32] (and also explored in Refs. [18,25,31,33]), based on light-front holographic QCD where the correct small Q^2 behavior (in order to simulate confinement) is introduced using the dressed current (see Ref. [32] for details).[7]

In this context, the TFF is defined as

$$F_{\pi^0\gamma^*\gamma}(Q^2) = \frac{P_{q\bar{q}}}{\pi^2 f_\pi}\int_0^1 \frac{dx}{(1+x)^2}\, x^{Q^2 P_{q\bar{q}}/(8\pi^2 f_\pi^2)}, \qquad \text{(A4)}$$

where $P_{q\bar{q}}$ is the probability of finding the $q\bar{q}$ component in the pion light-front wave function. To reproduce the anomaly $F_{\pi^0\gamma\gamma}(0) = 1/(4\pi^2 f_\pi)$, we impose $P_{q\bar{q}} = 0.5$.

[7]We do not consider higher-twist components to keep the model easy to use.

This model reproduces quite well the transition form factor data up to 10 GeV^2, but disagrees in particular with *BABAR*'s large Q^2 data (although compatible with Belle data within errors), especially because the model is reaching its asymptotic prediction ($Q^2 F_{\pi^0\gamma^*\gamma}(Q^2 \to \infty) = 2f_\pi$ [14]) already at this medium-Q^2 region. Another interesting feature of this model is that no convergence theorem from Padé theory is known for this kind of function, so the Padé convergence is not guaranteed in advance (in contrast to the previous Regge model). It represents a robustness test of our method.

After generating again a set of zero-error data points with the model of Eq. (A4), we use the PA sequence to fit these data and to obtain again the predictions for the a_i coefficients. We collect the results in Table V.

With the PA P_1^5 we obtain 0.04%, 4.6%, and 18.7% as a relative errors for a_0, a_1, and a_2, respectively. With the inclusion of the feasibility study at BES-III [42], we go down to 4.3% and 17.1% for a_1 and a_2, respectively. With the PTA sequence (the approximant pole located at $s_p = 1$ GeV^2), we obtain 0.6%, 4.8%, and 19.2%, respectively. Although no convergence theorem for this kind of function in Eq. (A4) is known, the convergence of our PA sequence is clear. That is one of the most interesting features of the PA methods: the convergence may occur beyond expectations.

[1] H. J. Behrend *et al.* (CELLO Collaboration), Z. Phys. C **49**, 401 (1991).
[2] J. Gronberg *et al.* (CLEO Collaboration), Phys. Rev. D **57**, 33 (1998).
[3] B. Aubert *et al.* (The *BABAR* Collaboration), Phys. Rev. D **80**, 052002 (2009).
[4] S. Uehara *et al.* (The Belle Collaboration), arXiv:1205.3249 [Phys. Rev. D (to be published)].
[5] S. L. Adler, Phys. Rev. **177**, 2426 (1969).
[6] J. S. Bell and R. Jackiw, Nuovo Cimento A **60**, 47 (1969).
[7] H. Fonvieille, N. Bensayah, J. Berthot, P. Bertin, M. Crouau, B. Bihoreau, G. Fournier, J. Miller *et al.*, Phys. Lett. B **233**, 65 (1989).
[8] F. Farzanpay, P. Gumplinger, A. Stetz, J. M. Poutissou, I. Blevis, M. Hasinoff, C. J. Virtue, C. E. Waltham *et al.*, Phys. Lett. B **278**, 413 (1992).
[9] R. Meijer Drees *et al.* (SINDRUM-I Collaboration), Phys. Rev. D **45**, 1439 (1992).
[10] E. Abouzaid *et al.* (KTeV Collaboration), Phys. Rev. Lett. **100**, 182001 (2008).
[11] K. Nakamura *et al.* (Particle Data Group), J. Phys. G **37**, 075021 (2010).
[12] P. Masjuan, S. Peris, and J. J. Sanz-Cillero, Phys. Rev. D **78**, 074028 (2008).
[13] J. J. Sanz-Cillero, arXiv:1002.3512; P. Masjuan, arXiv:1012.2806; P. Masjuan and J. J. Sanz-Cillero (to be published).
[14] G. P. Lepage and S. J. Brodsky, Phys. Rev. D **22**, 2157 (1980).
[15] G. A. Baker and P. Graves-Morris, *Encyclopedia of Mathematics and Its Applications* (Cambridge University Press, Cambridge, England, 1996).
[16] E. Ruiz Arriola and W. Broniowski, Phys. Rev. D **74**, 034008 (2006).
[17] E. R. Arriola and W. Broniowski, Phys. Rev. D **81**, 094021 (2010).
[18] S. V. Mikhailov and N. G. Stefanis, Nucl. Phys. **B821**, 291 (2009).
[19] A. E. Dorokhov, Phys. Part. Nucl. Lett. **7**, 229 (2010).
[20] A. V. Radyushkin, Phys. Rev. D **80**, 094009 (2009).
[21] M. V. Polyakov, JETP Lett. **90**, 228 (2009).
[22] H.-n. Li and S. Mishima, Phys. Rev. D **80**, 074024 (2009).
[23] S. Noguera and V. Vento, Eur. Phys. J. A **46**, 197 (2010).
[24] H. L. L. Roberts, C. D. Roberts, A. Bashir, L. X. Gutierrez-Guerrero, and P. C. Tandy, Phys. Rev. C **82**, 065202 (2010).
[25] S. S. Agaev, V. M. Braun, N. Offen, and F. A. Porkert, Phys. Rev. D **83**, 054020 (2011).
[26] Y. N. Klopot, A. G. Oganesian, and O. V. Teryaev, Phys. Lett. B **695**, 130 (2011).
[27] P. Kroll, Eur. Phys. J. C **71**, 1623 (2011).
[28] T. N. Pham and X. Y. Pham, Int. J. Mod. Phys. A **26**, 4125 (2011).
[29] M. Gorchtein, P. Guo, and A. P. Szczepaniak, Phys. Rev. C **86**, 015205 (2012).
[30] K. Kampf and J. Novotny, Phys. Rev. D **84**, 014036 (2011).
[31] S. J. Brodsky, F.-G. Cao, and G. F. de Teramond, Phys. Rev. D **84**, 033001 (2011).
[32] S. J. Brodsky, F.-G. Cao, and G. F. de Teramond, Phys. Rev. D **84**, 075012 (2011).
[33] A. P. Bakulev, S. V. Mikhailov, A. V. Pimikov, and N. G. Stefanis, Phys. Rev. D **84**, 034014 (2011).
[34] I. Balakireva, W. Lucha, and D. Melikhov, Phys. Rev. D **85**, 036006 (2012).
[35] H. Czyz, S. Ivashyn, A. Korchin, and O. Shekhovtsova, Phys. Rev. D **85**, 094010 (2012).
[36] C.-C. Lih and C.-Q. Geng, Phys. Rev. C **85**, 018201 (2012).
[37] D. Melikhov and B. Stech, Phys. Rev. D **85**, 051901 (2012).
[38] A. P. Bakulev, S. V. Mikhailov, A. V. Pimikov, and N. G. Stefanis, Phys. Rev. D **86**, 031501 (2012).
[39] P. Masjuan, Ph.D. thesis, Universitat Autònoma de Barcelona [arXiv:1005.5683].
[40] S. Peris, Phys. Rev. D **74**, 054013 (2006); P. Masjuan, J. J. Sanz-Cillero, and J. Virto, Phys. Lett. B **668**, 14 (2008); P. Masjuan and S. Peris, Phys. Lett. B **686**, 307 (2010).
[41] D. Babusci, H. Czyz, F. Gonnella, S. Ivashyn, M. Mascolo, R. Messi, D. Moricciani, A. Nyffeler, and G. Venanzoni, Eur. Phys. J. C **72**, 1917 (2012).
[42] B. Kloss, Bachelor thesis, University Mainz, 2011.
[43] I. Larin *et al.* (PrimEx Collaboration), Phys. Rev. Lett. **106**, 162303 (2011).
[44] J. Bijnens, A. Bramon, and F. Cornet, Z. Phys. C **46**, 599 (1990).
[45] K. Kampf, M. Knecht, and J. Novotny, Eur. Phys. J. C **46**, 191 (2006).
[46] H. R. Grigoryan and A. V. Radyushkin, Phys. Rev. D **77**, 115024 (2008).
[47] H. R. Grigoryan and A. V. Radyushkin, Phys. Rev. D **78**, 115008 (2008); S. K. Domokos, H. R. Grigoryan, and J. A. Harvey, Phys. Rev. D **80**, 115018 (2009).
[48] P. Colangelo, F. De Fazio, J. J. Sanz-Cillero, F. Giannuzzi, and S. Nicotri, Phys. Rev. D **85**, 035013 (2012).
[49] L. Cappiello, O. Cata, and G. D'Ambrosio, Phys. Rev. D **83**, 093006 (2011).
[50] M. Knecht and A. Nyffeler, Phys. Rev. D **65**, 073034 (2002).
[51] P. Masjuan, E. R. Arriola, and W. Broniowski, Phys. Rev. D **85**, 094006 (2012).
[52] C. Pommerenke, J. Math. Anal. Appl. **41**, 775 (1973); reviewed in G. A. Baker and P. Graves-Morris, *Encyclopedia of Mathematics and Its Applications* (Cambridge University Press, Cambridge, England, 1996), Sec. 6.5, Theorem 6.5.4, Corollary 1.
[53] P. Masjuan and S. Peris, J. High Energy Phys. 05 (2007) 040; P. Masjuan and S. Peris, Phys. Lett. B **663**, 61 (2008).